Available online at www.sciencedirect.com
ScienceDirect
Journal of the European Ceramic Society 27 (2007) 2445–2454
www.elsevier.com/locate/jeurceramsoc

Phase relationships and transport in Ti-, Ce- and Zr-substituted lanthanum silicate systems

Y.V. Pivak, V.V. Kharton *, A.A. Yaremchenko, S.O. Yakovlev, A.V. Kovalevsky, J.R. Frade, F.M.B. Marques

Department of Ceramics and Glass Engineering, CICECO, University of Aveiro, 3810-193 Aveiro, Portugal

Received 14 June 2006; received in revised form 28 August 2006; accepted 2 September 2006
Available online 18 October 2006

Abstract

The solubility of Ti^{4+} in the lattice of apatite-type $La_{9.83}Si_{6-x}Ti_xO_{26.75}$ corresponds to approximately 28% of the Si-site density. The conductivity of $La_{9.83}Si_{6-x}Ti_xO_{26.75}$ ($x = 1$–2) is predominantly oxygen-ionic and independent of the oxygen partial pressure in the $p(O_2)$ range from 10^{-20} to 0.3 atm. The electron transference numbers determined by the modified faradaic efficiency technique are lower than 0.006 at 900–950 °C in air. The open-circuit voltage of oxygen concentration cells with Ti-doped silicate electrolytes is close to the theoretical Nernst value both under oxygen/air and air/10%H_2–90%N_2 gradients at 700–950 °C, suggesting the stabilization of Ti^{4+} in the apatite structure. Titanium addition in $La_{9.83}Si_{6-x}Ti_xO_{26.75}$ ($x = 1$–2) leads to decreasing ionic conductivity and increasing activation energies from 93 to 137 kJ/mol, and enhanced degradation in reducing atmospheres due to SiO volatilization. At $p(O_2) = 10^{-20}$ atm and 1223 K, the conductivity decrease after 100 h was about 5% for $x = 1$ and 17% for $x = 2$. The solubility of Zr^{4+} in the $La_{9.83}Si_{6-x}Zr_xO_{26.75}$ system was found to be negligible, while the maximum concentration of Ce^{4+} in $La_{9.4-x}Ce_xSi_6O_{27-\delta}$ is approximately 5% with respect to the number of lanthanum sites.

Keywords: Electrical properties; Ionic conductivity; X-ray methods; Silicate; $La_{10}Si_6O_{27}$

1. Introduction

Oxygen ion-conducting solid electrolytes are key materials for numerous high-temperature electrochemical devices, including solid oxide fuel cells (SOFCs), oxygen pumps and sensors.[1–4] Developments of novel low-cost materials with the required transport and thermal properties and stability are of vital importance in this field. A relatively high level of oxygen ion transport in combination with moderate thermal expansion is observed for apatite-type silicates and germanates, $A_{10-x}(Si/GeO_4)_6O_{3-\delta}$, where A are the rare-earth and alkaline-earth metal cations.[5–18] Although Ge-based apatites have higher conductivity when compared to the analogous silicates,[7,16] the cost of Ge raw materials is higher and Ge is prone to volatilization at high temperatures.[14,16]

The apatite structure of silicates consists of isolated SiO_4 tetrahedra and A-site cations, occupying cavities between SiO_4 units; additional oxygen sites (O4) surrounded by La2 cations (S.G. $P6_3/m$) form channels running through the *c*-axis of the lattice (Fig. 1). The conductivity data on apatite systems and the results of atomistic modelling, structural refinement and Mössbauer spectroscopy (e.g. [8,12–15] and references therein) clearly show that interstitial migration of oxygen ions along these channels is a key contribution to the overall ionic transport. A-site vacancies are another important factor affecting the ionic conductivity in the apatites particularly when in positions enveloping oxygen channels. A-site deficiency influences the SiO_4 tetrahedra relaxation and may cause displacement of the anions from channel into new interstitial sites, thus creating vacancies at fixed oxygen content.[11,12,15,17] The oxygen stoichiometry may, thus, determine the level of ionic transport in apatites; this suggests guidelines to enhance the transport properties by suitable composition changes, namely by partial substitutions with cations of higher valency. A wide range of substitution possibilities of Si, as well as of A-site cations, gives a

* Corresponding author. Tel.: +351 234 370263; fax: +351 234 425300.
E-mail address: kharton@cv.ua.pt (V.V. Kharton).

0955-2219/$ – see front matter © 2006 Elsevier Ltd. All rights reserved.
doi:10.1016/j.jeurceramsoc.2006.09.004

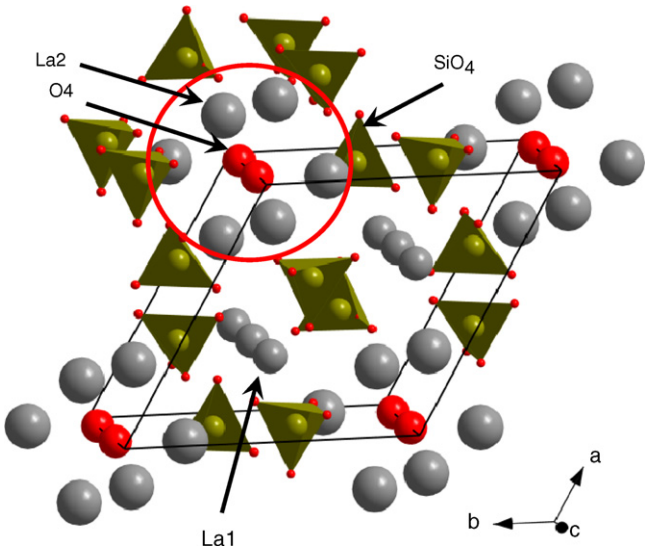

Fig. 1. Crystal structure of $La_{9.83}Si_{6-x}Ti_xO_{26.75}$ apatite (S.G. $P6_3/m$).

huge potential for modifying and even, in some cases, improving the ionic transport properties of apatite-type silicates. A range of cations (Al, Ga, Fe, Mn, Co, Ti, Mg) already were successfully incorporated into the tetrahedral site of the apatite lattice.[10,19–24]

At the same time, the apatite-type silicate systems are also characterized by moderate stability in reducing environments at elevated temperatures.[19,20] The long-term stability tests of apatite-type $La_{10-x}Si_{6-y}Al_yO_{27-3x/2-y/2}$ ceramics in reducing atmospheres demonstrated a slow irreversible degradation of these silicates at temperatures above 800 °C, associated with reduction to SiO and its volatilization from the surface layers.[19] Decreasing operating temperature of electrochemical cells down to approximately 500–750 °C is needed to avoid silicon oxide volatilization.[19]

Another effective way to try to circumvent volatilization is doping on the Si-site. One may select different strategies, namely interaction of the redox pair Si^{4+}/Si^{2+} with other redox pairs, and also attempts to suppress the reducibility of SiO_2 in apatites by lowering its content and chemical activity. In spite of a recent investigation on Ti-doping by Sansom et al.,[23] information on the stability of the apatite lattice in reducing conditions as well as on ionic and electronic contributions is scarce. Therefore, a deeper understanding of the influence of Ti^{4+}/Ti^{3+} ions on the transport properties of apatite silicates is required. To our knowledge, there are no published data on Zr doping on the B-site. Information on Ce-substituted apatites is also very limited. It the latter case, if feasible, a range of compositions with constant A-site deficiency and variable concentrations of oxygen interstitials might be exploited. Lastly, this information might also be desirable to assess the chemical compatibility of silicate apatites with other ion-conducting materials based on zirconia and ceria used as components of multiphase electrodes in several electrochemical devices.[2,3]

Considering the above mentioned comments, the aim of this work was the assessment of the solubility of tetravalent cations (Ti, Ce, Zr) in apatite-type silicates and to study the effects of doping on properties relevant for practical applications.

2. Experimental

$La_{9.83}Si_{6-x}M_xO_{26.75}$ (M = Ti, Zr; x = 1–2) and $La_{9.4-x}Ce_xSi_6O_{27-\delta}$ (x = 1–3) were synthesized from high purity La_2O_3, SiO_2, TiO_2, ZrO_2 and $Ce(NO_3)_3$ via a conventional solid-state route. Before weighing, lanthanum oxide and silica were annealed in air at 1200 °C and 600 °C, respectively. The stoichiometric mixtures were ball-milled and reacted at 1000 °C and 1200 °C for 4 h in air and repeatedly milled. The powders were uniaxially pressed at 50–100 MPa into disks of various thicknesses. Gas-tight ceramics were sintered at 1600–1700°C for 10 h in air. Experimental densities of Ti-doped apatites were higher than 91% of their theoretical density calculated from XRD data (Table 1). After sintering, the ceramics were annealed in air at 1000 °C for 3 h and slowly cooled (2–3 K/min) to obtain equilibrium oxygen content.

X-ray diffraction (XRD) patterns were collected at room temperature using a Rigaku D/MAX-B diffractometer (Bragg–Brentano geometry, Cu Kα radiation) in the 2θ angle range 5–100° with a step of 0.02° and average time of 8 s per step. For structural analysis, the FullProf program[25] was employed. The crystal structures were refined using the full profile Rietveld method including the refinement of lattice parameters, positional and thermal parameters, occupancy parameters, scaling factor, zero shift, background function and Bragg-peak profile parameters. A Hitachi S-4100 scanning electron microscope (SEM) with a Rontec UHV detection system for energy dispersive spectroscopy (EDS) was used for microstructural studies. Thermal expansion was studied in air using a Linseis L70 dilatometer (heating rate of 5 K/min). The temperature dependencies of total conductivity (σ) in flowing air and 10%H_2–90%N_2 mixture were investigated by AC impedance spectroscopy (HP4284A precision LCR meter, 20 Hz–1 MHz): the oxygen partial pressure in the measuring cell was determined using a yttria-stabilized zirconia (YSZ) oxygen sensor. The isothermal measurements of total conductivity and Seebeck coefficients at 700–950 °C were

Table 1
Properties of Ti-containing apatite ceramics

Composition	Phase impurities	ρ_{exp} (g/cm^3)	ρ_{calc} (g/cm^3)	Relative density (%)	Average TECs	
					T (K)	$\bar{\alpha} \times 10^6$ (K^{-1})
$La_{9.83}Si_5TiO_{26.75}$	–	5.57	5.766	96.6	100–1150	9.74 ± 0.01
$La_{9.83}Si_4Ti_2O_{26.75}$	P′ (4%)	5.37	5.624	91.6	100–1150	10.26 ± 0.01

Notes: ρ_{exp} and ρ_{calc} are the experimental and calculated density of materials, respectively; P′ corresponds to the $La_2Ti_2O_7$ pyrochlore phase (S.G. $Pna2_1$).

carried out in the oxygen partial pressure range 10^{-20} to 0.3 atm as described elsewhere.[26]

The oxygen ion transference numbers were determined by modified electromotive force (EMF) and faradaic efficiency (FE) methods, taking electrode polarization into account. Detailed description of the experimental procedures can be found elsewhere.[27–29] The FE experiments were carried out under zero oxygen chemical potential gradient in air at 900 °C and 950 °C. The determination of the average oxygen ion transference number by the modified EMF technique was performed at 700–950 °C under O_2/air and air/10%H_2–90%N_2 gradients, with continuous monitoring of the oxygen partial pressure in the gas mixtures by electrochemical oxygen sensors.

3. Results and discussion

3.1. Selected phase relationships

The XRD patterns of apatite-type $La_{9.4-x}Ce_xSi_6O_{27-\delta}$ ceramics are shown in Fig. 2A–C. Doping with even a relatively small amount of Ce ($x=1$) leads to the segregation of about 4 wt% of CeO_2. This suggests that the maximum solubility of Ce ions in the apatite lattice is close to 5.5% of the density of lanthanum sites, i.e. about 0.5 atoms per formula unit. Notice also that XRD patterns of Ce-doped apatites with $x=1$–2 displayed peak shifts to higher angles (Fig. 2A and B) due to a decrease in the unit cell volume, confirming the incorporation of Ce^{4+} cations with a smaller cation radius[30] in the lanthanum sites; this effect cannot be ascribed to increasing A-site deficiency or Si^{4+} substitution, which are expected to expand the lattice. Increasing Ce concentration results in the appearance of additional peaks of La_2O_3, SiO_2 and, at $x=3$, $La_2Si_2O_7$. This observation prevented the exploitation of significant doping levels and justified the limited attention dedicated to the electrical characterization of these materials.

XRD characterization of $La_{9.83}Si_{6-x}Zr_xO_{26.75}$ ($x=1$–2) materials showed a negligible solubility of Zr^{4+} cations due to $La_2Zr_2O_7$ pyrochlore formation. Inspection of the XRD pattern of $La_{9.83}Si_5ZrO_{26.75}$ revealed also the presence of other impurity phases, including ZrO_2, SiO_2, La_2O_3 and $ZrSiO_4$, probably metastable. Whatever the formation mechanism of these impurities, the ratio of strongest reflections of the apatite and $La_2Zr_2O_7$ phases was 1:0.7 and 0.35:1 for $x=1$ and 2, respectively (Fig. 2D and E). Thus, additions of zirconia lead to complete decomposition of apatite solid solutions due to the formation of $La_2Zr_2O_7$, which is the most thermodynamically stable phase in the ZrO_2–La_2O_3 binary system.[31] As lanthanum zirconate has insulating properties and blocks ionic transport,[31] the use of zirconia-based components in electrodes applied onto silicate-based ceramics should be avoided.

In contrast to Zr- and Ce-containing systems, $La_{9.83}Si_5TiO_{26.75}$ was found single-phase; in the case of $La_{9.83}Si_4Ti_2O_{26.75}$, minor extra peaks corresponding to the pyrochlore $La_2Ti_2O_7$ were observed (Fig. 3). The onset of phase

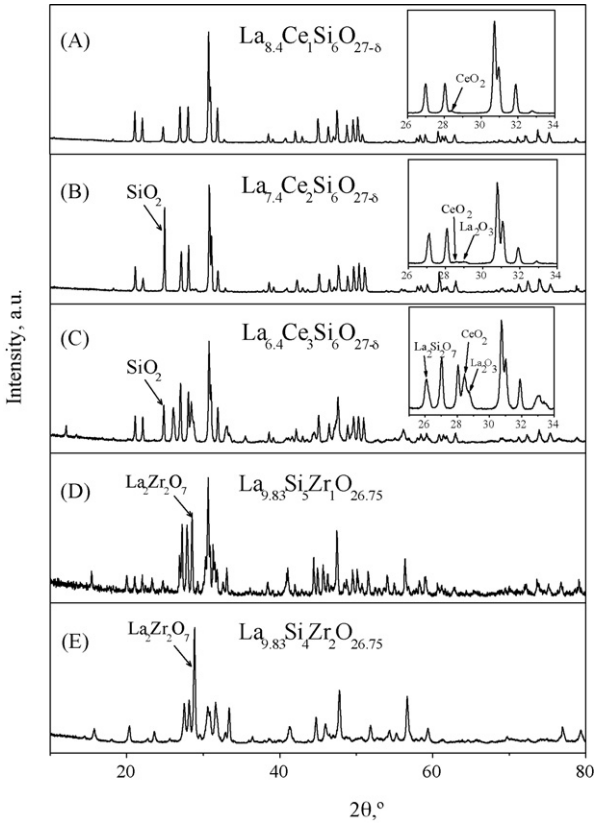

Fig. 2. XRD patterns of Zr- and Ce-containing silicate systems. The insets and arrows show phase impurity reflexes.

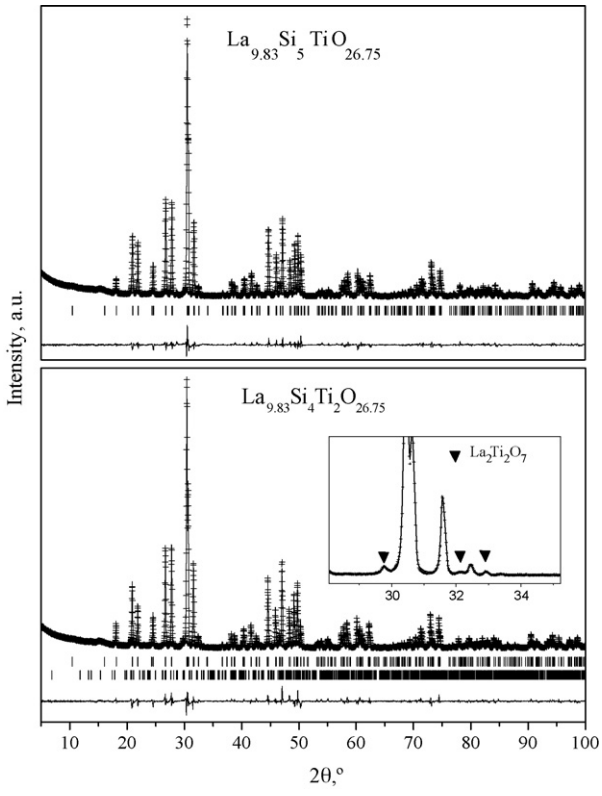

Fig. 3. Rietveld refinement results of the $La_{9.83}Si_{6-x}Ti_xO_{26.75}$ ceramics. Experimental and calculated patterns, difference profile and the position of diffraction maxima are given. Inset shows the peaks of $La_2Ti_2O_7$ pyrochlore.

impurities can be understood by taking into account that the cation to anion size ratio (r_{Ti}:$r_O \approx 0.46$) is already slightly above the typical values of MO_4 tetrahedra. Besides the positive identification of the phase impurities now provided, these results are in good agreement with data reported by Sansom et al.[23] Note that apatite-type germanates exhibit a higher solubility of Ti^{4+} in the lattice when compared with the analogous Si-containing systems, possibly due to closer proximity between r_{Ti}:$r_O \approx 0.46$ and r_{Ge}:$r_O \approx 0.36$ compared to r_{Si}:$r_O \approx 0.28$. For instance, the apatite-type $La_{9.33}Ge_4Ti_2O_{26}$ is a single-phase material, while attempts to increase the Ti content further up to 50% exceeded the solubility limit.[23] Nonetheless, the solubility of Ti^{4+} cations in $La_{9.83}Si_{6-x}Ti_xO_{26.75}$ system is high enough to assess the effects of substitution on the apatite structure and electrical properties.

3.2. Crystal structure of Ti-containing apatites

The refinement of XRD patterns of $La_{9.83}Si_{6-x}Ti_xO_{26.75}$ was performed in the rhombohedral *P*-3 and hexagonal $P6_3$ and $P6_3/m$ space groups; the final selection of space group was based on the agreement factors. The best agreement between the experimental and calculated profiles was found for the hexagonal space group $P6_3/m$. In the case of $La_{9.83}Si_4Ti_2O_{26.75}$, the $La_2Ti_2O_7$ pyrochlore phase was also included in the refinement procedure; the estimated weight fractions were 96 and 4% for the apatite and pyrochlore phases, respectively (Table 1). The final structural data are summarized in Tables 2 and 3; graphical results of the Rietveld refinement are presented in Fig. 3. The incorporation of Ti^{4+} with a larger ionic radius if compared to Si^{4+}[30] increases the unit cell parameters and volume (Table 2), as observed for doping with Al^{3+}, Fe^{3+}, Ga^{3+} and Ge^{4+}.[10,13,15,16] The refined composition of the apatite solid solution in the two-phase $La_{9.83}Si_4Ti_2O_{26.75}$ ceramics can be written as $La_{9.5}Si_4Ti_{1.67}O_{25.6}$; the solubility limit of Ti^{4+} can therefore be estimated as 28% of the silicon site density.

In the course of the refinement, site occupancy and atomic displacement parameters (adp) were taken into account, while only the isotropic displacement parameters were employed. According to the results, cation vacancies are located in La1 sites, in good agreement with our previous results;[13] the La2 sites remain fully occupied (Table 2). One should mention that La2 atoms form the oxygen channels (Fig. 1), responsible for high oxygen-ionic conductivity in the apatite systems.[12–15] The occupancy of the Si/Ti site was found close to the nominal one, e.g. 0.83/0.17 for $La_{9.83}Si_5TiO_{26.75}$ and 0.72/0.28 for $La_{9.83}Si_4Ti_2O_{26.75}$ ceramics. As the conventional X-ray diffraction analysis is not sufficiently sensitive to lightweight atoms, the calculated values of oxygen-site occupancies must be considered equal to unity. In general, the refined cation compositions of the Ti-doped apatite ceramics are in reasonable agreement with expectation within normal limits of calculation errors (Table 2). Another necessary comment is that the displacement parameters of the channel oxygen O4 are quite high, thus indicating a considerable level of disorder in these channels. Though the unit cell volume increases with Ti content in $La_{9.83}Si_{6-x}Ti_xO_{26.75}$, probably due to the increasing size of TiO_4 tetrahedra, this results in narrower oxygen channels that might cause both a higher potential barrier for the transport of interstitial oxygen and decreasing oxygen-ionic conductivity.

Table 2
Crystallographic data of $La_{9.83}Si_{6-x}Ti_xO_{26.75}$

Atom (sites)	Parameters	$La_{9.83}Si_{6-x}Ti_xO_{26.75}$	
		$x=1$	$x=2$
	a/b (Å)	9.7787(2)	9.8074(2)
	c (Å)	7.2380(2)	7.2553(2)
	V (Å^3)	599.39(12)	604.36(12)
La1 (4f) (1/3, 2/3, z)	z	−0.0011(5)	−0.0008(6)
	Site occ.	0.95(4)	0.98(3)
	U_{iso} (×100)	1.31(5)	1.2(4)
La2 (6h) (x, y, 1/4)	x	0.2308(3)	0.2303(2)
	y	−0.0114(6)	−0.0097(5)
	Site occ.	1.01(3)	1.00(4)
	U_{iso} (×100)	0.92(5)	0.84(5)
Si/Ti (6h) (x, y, 1/4)	x	0.4044(5)	0.4073(5)
	y	0.3773(6)	0.3792(4)
	Site occ.	0.84(5)/0.16(5)	0.69(5)/0.31(5)
	U_{iso} (×100)	1.41(6)	1.16(4)
O1 (6h) (x, y, 1/4)	x	0.330(2)	0.331(3)
	y	0.488(2)	0.499(2)
	Site occ.	1.00(6)	1.0(4)
	U_{iso} (×100)	0.89(5)	1.93(3)
O2 (6h) (x, y, 1/4)	x	0.593(2)	0.590(2)
	y	0.463(2)	0.467(2)
	Site occ.	1.06(5)	1.01(5)
	U_{iso} (×100)	0.60(6)	2.71(5)
O3 (12i) (x, y, z)	x	0.349(2)	0.347(2)
	y	0.261(1)	0.260(1)
	z	0.059(1)	0.075(1)
	Site occ.	1.04(5)	1.04(4)
	U_{iso} (×100)	2.44(3)	1.37(5)
O4 (2a) (0, 0, 1/4)	Site occ.	1.01(5)	0.99(4)
	U_{iso} (×100)	3.44(6)	2.68(5)
	Rp	6.33%	7.16%
	Rwp	8.65%	9.82%

Table 3
Selected bond distances of Ti-containing apatite phases

Bond	$La_{9.83}Si_5TiO_{26.75}$, distance (Å)	$La_{9.83}Si_4Ti_2O_{26.75}$, distance (Å)
La1—O1 [×3]	2.508(8)	2.443(9)
La1—O2 [×3]	2.508(9)	2.555(7)
La1—O3 [×3]	2.847(7)	2.897(8)
La2—O1	2.830(7)	2.898(6)
La2—O2	2.594(6)	2.577(8)
La2—O3 [×2]	2.423(7)	2.536(7)
La2—O3 [×2]	2.699(8)	2.628(9)
La2—O4	2.314(2)	2.308(3)
Si/Ti—O1	1.580(5)	1.682(7)
Si/Ti—O2	1.600(4)	1.556(5)
Si/Ti—O3 [×2]	1.697(6)	1.623(6)

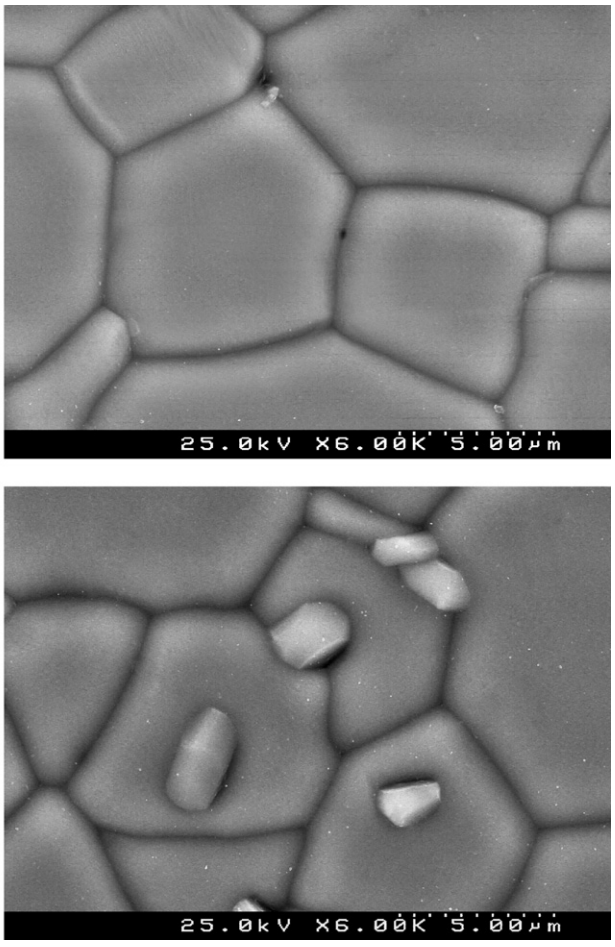

Fig. 4. SEM micrographs of $La_{9.83}Si_5TiO_{26.75}$ (A) and $La_{9.83}Si_4Ti_2O_{26.75}$ (B) ceramics.

3.3. Microstructure, thermal expansion and total conductivity of Ti-containing ceramics

SEM studies showed the high quality of $La_{9.83}Si_5TiO_{26.75}$ ceramics, in particular a low porosity and the absence of compositional inhomogeneities along the grain boundaries. This conclusion quite well agrees with the ratio between experimental and theoretical density for this material, 96.6% (Table 1). The $La_{9.83}Si_4Ti_2O_{26.75}$ ceramics have a similar grain size, while the segregation of $La_2Ti_2O_7$ is clearly visible in the SEM micrographs (Fig. 4). In the latter case, the density is 91.6% of theoretical, calculated taking into account the cation composition and the pyrochlore impurity content obtained from the XRD data.

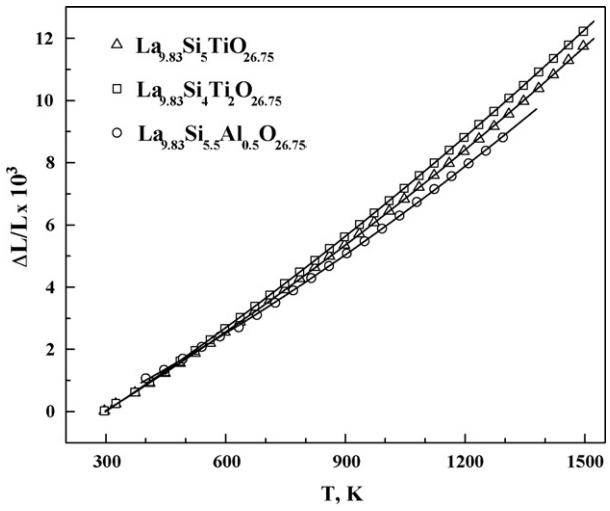

Fig. 5. Dilatometric curves of apatite ceramics in air.

Fig. 5 presents the dilatometric curves of $La_{9.83}Si_{6-x}Ti_xO_{26.75}$ in air; the dilatometric data on $La_{9.83}Si_{5.5}Al_{0.5}O_{26.75}$ with similar oxygen content[19] are given for comparison. The average thermal expansion coefficients (TECs) at 150–1150 °C are relatively low, $(9.7–10.3) \times 10^{-6}\,K^{-1}$ (Table 1) and close to those of commonly used solid electrolytes, such as yttria-stabilized zirconia.[31]

Fig. 6 shows two selected impedance spectra of $La_{9.83}Si_{6-x}Ti_xO_{26.75}$ ceramics, at 750 °C. The spectra consisting of two arcs were observed for both Ti-containing materials in the temperature range 650–1000 °C. The specific capacitance varied in the narrow range $(3–4) \times 10^{-9}$ F/cm for the high-frequency response and $(3–5) \times 10^{-4}$ F/cm for the low-frequency response. The low-frequency response can be

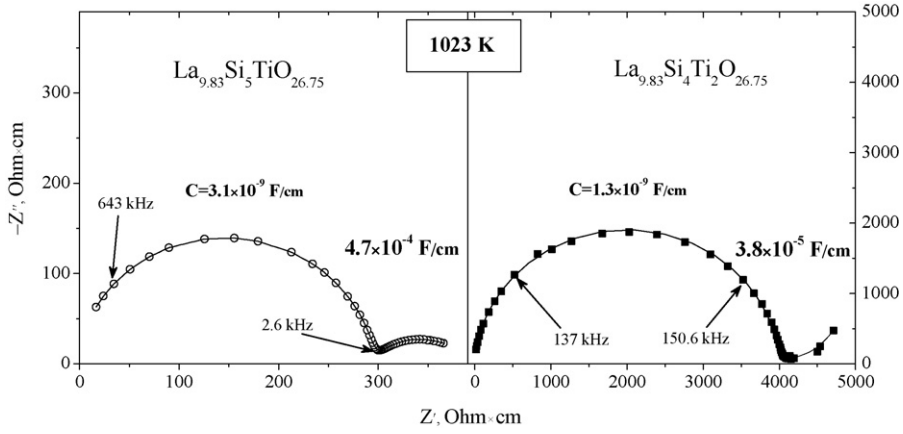

Fig. 6. Examples of impedance spectra of $La_{9.83}Si_{6-x}Ti_xO_{26.75}$ ceramics with porous Pt electrodes in air. Solid lines correspond to the fitting results. The specific capacitances (C) are given near the corresponding parts of the spectra.

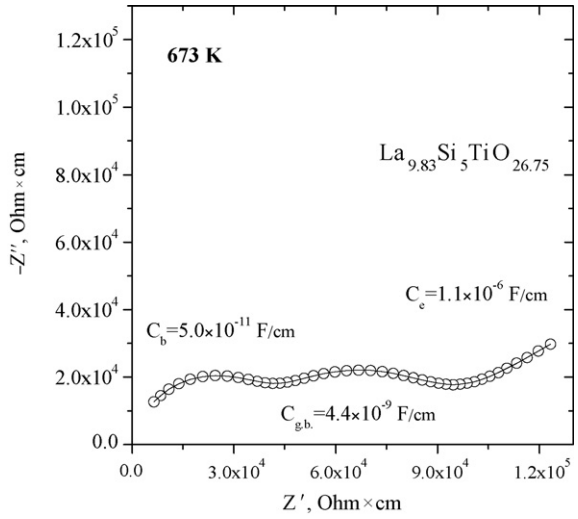

Fig. 7. Example of the impedance spectra of $La_{9.83}Si_5TiO_{26.75}$ with porous Pt electrodes in air, illustrating the separation of bulk, grain boundary and electrode signals. Solid lines correspond to the fitting results.

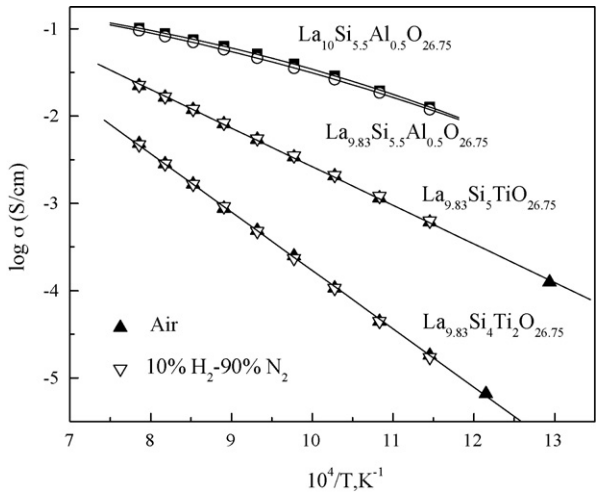

Fig. 9. Temperature dependences of the total conductivity of the apatite ceramics in air and dry 10%H_2–90%N_2 flows. The data on Al-doped apatite ceramics[19] are shown for comparison.

clearly ascribed to the electrode process; the corresponding intercept of this arc at intermediate frequencies defines the total (bulk and grain boundary) resistance. Note that the values of dielectric constant extracted from the capacitance at high frequency are in the range 100–500, that is about one order of magnitude higher that expected for solid electrolytes.

At lower temperatures, 300–500 °C, the grain-boundary resistivity can be separated from the bulk contribution as evidenced by the impedance spectra shown in Fig. 7. The temperature dependencies of the bulk, grain boundary and total conductivities are illustrated in Fig. 8; the corresponding activation energies (E_a) were calculated by the standard Arrhenius equation. As for other solid-electrolyte materials (e.g.[31] and references cited), the E_a value for the ceramics bulk (91 kJ/mol) is considerably lower than for grain boundaries (114 kJ/mol).

Fig. 9 compares the total conductivity of $La_{9.83}Si_{6-x}Ti_xO_{26.75}$ and $La_{9.83}Si_{5.5}Al_{0.5}O_{26.75}$ in air (filled symbols) and in 10%H_2–90%N_2 gas mixture flow (open symbols). Doping with titanium leads to drastic decrease of conductivity and an increase in the activation energy (Table 4), as expected from structural data. The total conductivity of Ti-substituted apatites remains essentially $p(O_2)$-independent. This indicates a predominant ionic conductivity, in agreement with the FE and EMF data discussed below. The presence of $La_2Ti_2O_7$ as a secondary phase may only have a minor effect on transport properties. In fact, the total conductivity of $La_2Ti_2O_7$ pyrochlore phase is approximately 10^{-5} S/cm at 530 °C,[32] considerably lower than that observed for the corresponding apatite systems. On the other hand, the activation energy of $La_2Ti_2O_7$, 120.6 kJ/mol,[32] is comparable with the E_a value characteristic of $La_{9.83}Si_4Ti_2O_{26.75}$ ceramics.

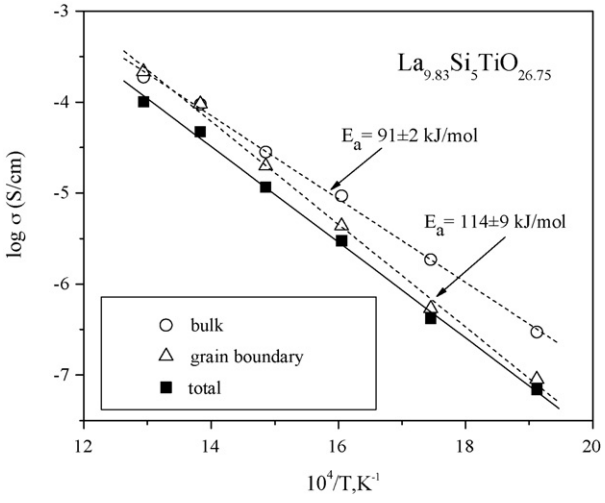

Fig. 8. Temperature dependences of bulk, grain boundary and total conductivities of $La_{9.83}Si_5TiO_{26.75}$ in air.

The long-term stability tests in reducing atmospheres showed an irreversible degradation of these materials at 950 °C, as for other apatite systems.[19,20] For $La_{9.83}Si_5TiO_{26.75}$, the conductivity drop in flowing H_2–N_2 mixture is about 5.5% after 100 h; for $La_{9.83}Si_4Ti_2O_{26.75}$, this value is approximately three times larger, 17.5% (Fig. 10). This suggests that degradation under reducing conditions becomes worse with increasing titania content. XRD inspection of the $La_{9.83}Si_5TiO_{26.75}$ after long-term treatment in reducing environment revealed the presence of small amounts of lanthanum and, possibly silicon oxides (Table 5); due to the small intensity of the impurity peaks exact identification is impossible.

Table 4
Activation energy for the total conductivity in different atmospheres

Composition	E_a (kJ/mol)		Ref.
	Air	10%H_2–90%N_2	
$La_{9.83}Si_5TiO_{26.75}$	92.7 ± 0.6	91.4 ± 0.6	This work
$La_{9.83}Si_4Ti_2O_{26.75}$	137 ± 2	138.6 ± 0.6	This work
$La_{9.83}Si_{5.5}Al_{0.5}O_{26.5}$	57 ± 3	55 ± 3	[20]
$La_{10}Si_{5.5}Al_{0.5}O_{26.75}$	56 ± 4	62 ± 3	[20]

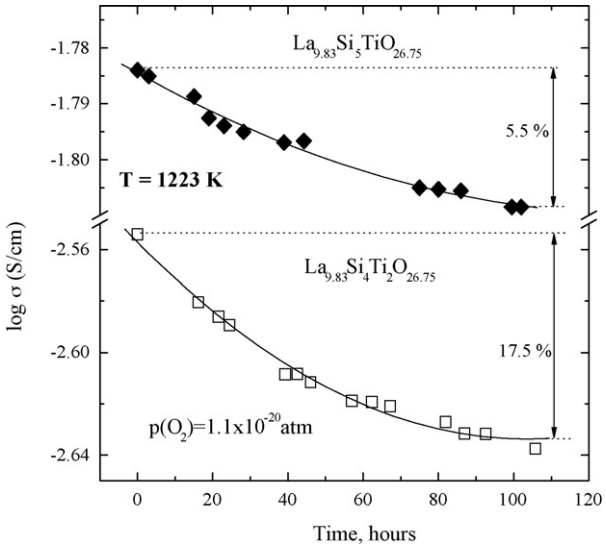

Fig. 10. Time dependences of the total conductivity of apatite ceramics in flowing 10%H_2–90%N_2 mixture at 950 °C. The oxygen partial pressure is 1.1×10^{-20} atm.

In the case of $La_{9.83}Si_4Ti_2O_{26.75}$, the XRD analysis detected only an increase of the weight fraction of the pyrochlore phase (P′) up to 6%. Most likely, a minor volatilization of silicon oxide increases the lanthanum activity in the apatite solid solution and promotes the formation of $La_2Ti_2O_7$. This effect seems responsible for the fast degradation of $La_{9.83}Si_4Ti_2O_{26.75}$ ceramics (Fig. 10). The SiO volatilization leads also to a lattice contraction due to decreasing La-site deficiency, as shown in Table 5.

SEM inspection combined with chemical analysis of these materials suggests that the conductivity drop is mainly related to changes in the outside layers, near the exposed surface, where significant morphological alterations are observed (Fig. 11). In the bulk of dense apatite ceramics, where Si^{4+} depletion hardly takes place microstructural changes were absent.

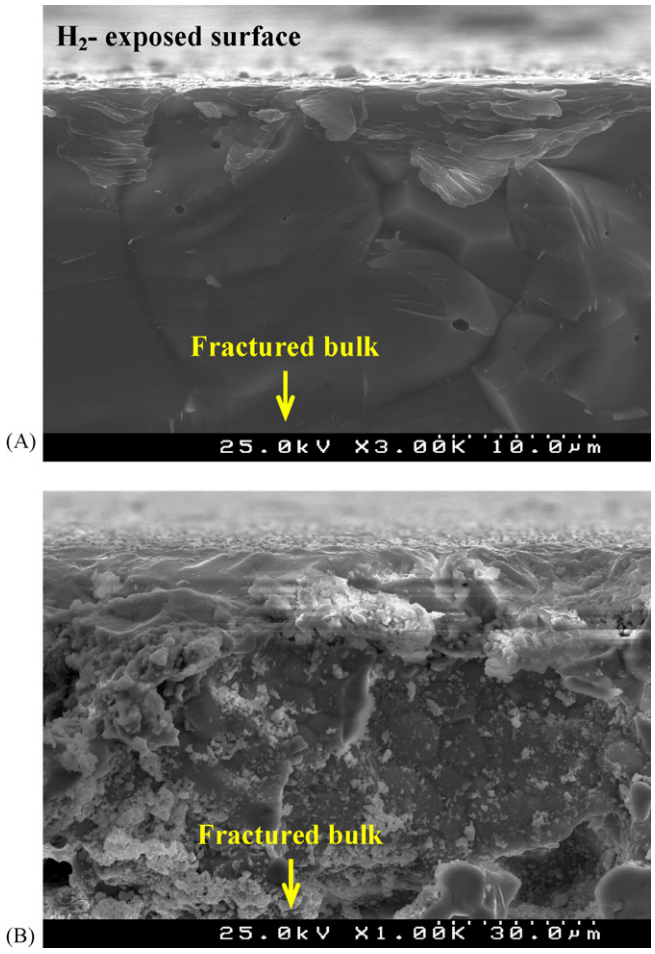

Fig. 11. SEM micrographs of $La_{9.83}Si_5TiO_{26.75}$ (A) and $La_{9.83}Si_4Ti_2O_{26.75}$ (B) ceramics after 100 h degradation tests in H_2-containing atmosphere.

3.4. Oxygen-ionic transport

The oxygen pressure dependences of the total conductivity and Seebeck coefficient (α) of $La_{9.83}Si_{6-x}Ti_xO_{26.75}$ (Figs. 12 and 13) are typical for solid oxide electrolytes. In particular, under oxidizing conditions the slope of the α versus $\ln p(O_2)$ dependencies is close to $-R/4F$, the theoretical value for pure oxygen-ionic conductors.[33] A similar behavior was reported earlier for other apatite-type systems.[10,13,22] Under reducing conditions, the behavior of Seebeck coefficient becomes more complex. The deviation from linear α versus $\ln p(O_2)$ dependencies at low oxygen chemical potentials may be associated either with silicon oxide volatilization from silicate surface, or with a minor n-type contribution due to reduction of Ti^{4+} to Ti^{3+}. Note that the deviations from linearity increase with the Ti content (Fig. 13). However, this still corresponds to minor conductivity contributions because total conductivity is almost independent of the oxygen partial pressure down to 10^{-20} atm.

The EMF and FE measurements confirmed that the apatite-type $La_{9.83}Si_{6-x}Ti_xO_{26.75}$ is a solid electrolyte with negligible electronic contribution. The experimental EMF values of the oxygen concentration cells (E_{exp}) are quite close to the theoretical Nernst values ($E_{theoretical}$), both under O_2/air and under air/10%H_2–90%N_2 gradients (Figs. 14 and 15). The modified FE technique showed that the electronic contribution to the total conductivity in air is lower than 0.6% (Table 6).

Table 5
XRD data on $La_{9.83}Si_{6-x}Ti_xO_{26.75}$ ceramics (x = 1–2) after degradation in 10%H_2–90%N_2 mixture during 105 h

Nominal composition	Phase impurities	Lattice parameters		V (Å^3)
		a (Å)	c (Å)	
$La_{9.83}Si_5TiO_{26.75}$	La_2O_3 or SiO_2 (<5%)	9.7776(3)	7.2331(3)	598.85(12)
$La_{9.83}Si_4Ti_2O_{26.75}$	P′ (6%)	9.8057(2)	7.2497(3)	603.68(12)

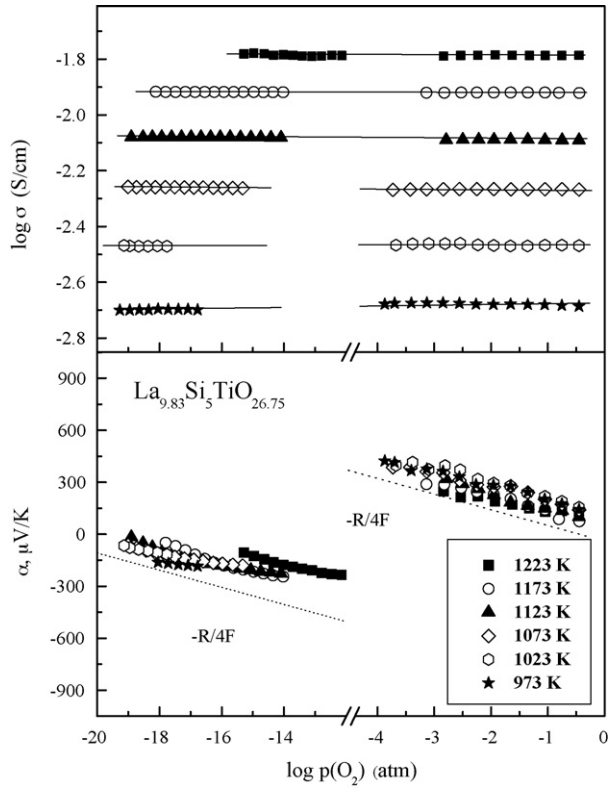

Fig. 12. Oxygen pressure dependencies of the total conductivity and Seebeck coefficient of $La_{9.83}Si_5TiO_{26.75}$.

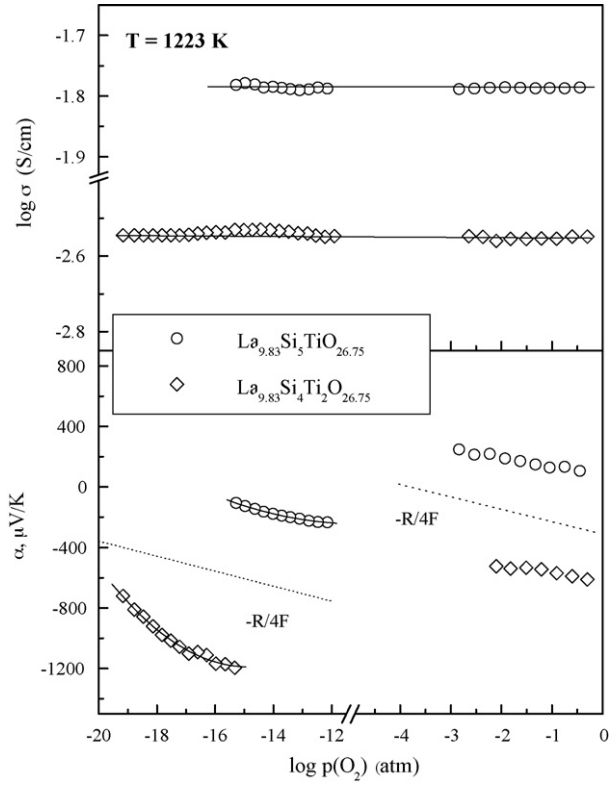

Fig. 13. Oxygen pressure dependencies of the total conductivity and Seebeck coefficient of Ti-doped apatite ceramics at 950 °C.

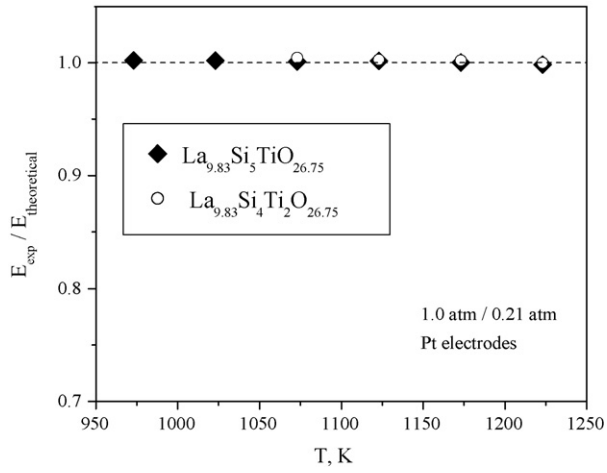

Fig. 14. Ratio between experimental and theoretical EMF of the oxygen concentration cells with $La_{9.83}Si_{6-x}Ti_xO_{26.75}$ electrolytes, placed under the oxygen partial pressure gradient of 1.0 atm/0.21 atm.

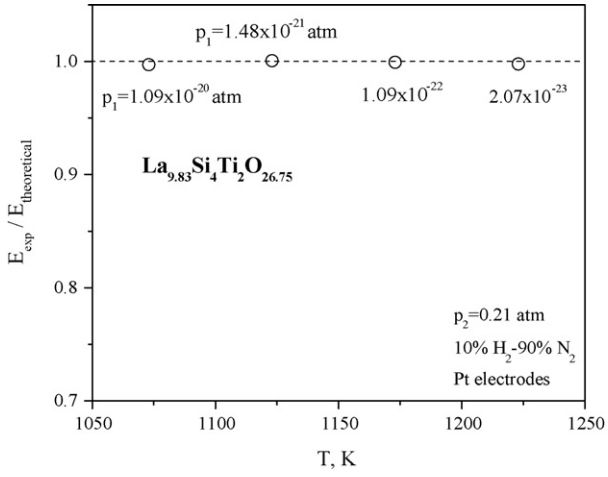

Fig. 15. Ratio between experimental and theoretical EMF of the oxygen concentration cells with $La_{9.83}Si_4Ti_2O_{26.75}$ electrolyte placed under air/H_2–H_2O–N_2 gradient, as function of temperature. The oxygen partial pressure in hydrogen-containing mixtures (p_1) is given near the experimental data points.

The decrease of ionic conductivity on Ti doping (Fig. 9) may result from local lattice distortion near the relatively large Ti^{4+}.[30] However, the actual mechanisms may differ from the inhibition of ionic migration in different structural types, namely zirconia-based fluorite (YSZ) and perovskite-type $La(Sr)GaO_{3-\delta}$.[34–36] Raman spectroscopy studies of Ti-doped YSZ demonstrated that a decrease in ionic transport occurs due to trapping of oxygen vacancies near Ti^{4+} by shifting the coordination from eightfold

Table 6
Oxygen-ion transference numbers of $La_{9.83}Si_5TiO_{26.75}$ determined by the FE measurements in air

T (K)	U (mV)	Oxygen-ion transport number
1223	959	0.9963
	644	0.9963
1173	428	0.9942
	1028	0.9966

to sixfold.[35] In the case of $La_{0.86}Sr_{0.14}Ga_{0.96}Ti_{0.04}O_{3-\delta}$, a decrease in ionic conductivity was attributed to a lower ion mobility caused by strong coulombic attraction between Ti^{4+} and neighboring O^{2-} anions.[36] In the title materials, ionic conduction is probably affected by strong lattice distortion caused by large TiO_4 tetrahedra, thus narrowing the migration channels.

4. Conclusions

The maximum solubility of Ce^{4+} in the lanthanum sublattice of $La_{9.4-x}Ce_xSi_6B_{27-\delta}$ is low, close to 5.5% of the La-site concentration. Further additions of ceria lead to the segregation of CeO_2. While this result prevents a deeper study of this system, it also suggests that apatite-type silicate electrolytes and Ce-containing electrode materials are chemically compatible in high-temperature electrochemical cells. On the contrary, zirconia additions result in decomposition of the apatite phase and formation of insulating $La_2Zr_2O_7$, indicating that the use of zirconia-containing electrodes in contact with $La_{10-x}Si_6O_{27}$-based solid electrolytes should be avoided. The solubility of Ti^{4+} cations in $La_{9.83}Si_{6-x}Ti_xO_{26.75}$ system is substantially high, up to 28% of the Si-site concentration. The conductivity of Ti-substituted apatites is predominantly oxygen-ionic and independent of the oxygen partial pressure in the range 10^{-20} to 0.3 atm, revealing a stabilization of Ti^{4+} oxidation state in the apatite lattice. However, doping with titanium decreases the ionic transport and promotes degradation in reducing atmospheres due to segregation of $La_2Ti_2O_7$ pyrochlore. This shows that silicate doping strategies based on the use of lower-valence cations, such as Al^{3+}, still provide the best results.

Acknowledgements

This work was partially supported by the FCT, Portugal (projects SFRH/BPD/24639/2005 and SFRH/BPD/15003/2004, and POCI program), and the MatSILC project (STRP 033410, CEC).

References

1. Badwal, S. P. S. and Ciacchi, F. T., Ceramic membrane technologies for oxygen separation. *Adv. Mater.*, 2001, **13**, 993–996.
2. Steele, B. C. H., Material science and engineering: the enabling technology for the commercialisation of fuel cell systems. *J. Mater. Sci.*, 2001, **36**, 1053–1068.
3. Yamamoto, O., Solid oxide fuel cells: fundamental aspects and prospects. *Electrochim. Acta*, 2001, **45**, 2423–2441.
4. Dyer, P. N., Richards, R. E., Russek, S. L. and Taylor, D. M., Ion transport membrane technology for oxygen separation and syngas production. *Solid State Ionics*, 2000, **134**, 21–33.
5. Nakayama, S., Kageyama, T., Aono, H. and Sadaoka, Y., Ionic conductivity of lanthanoid silicates, $Ln_{10}(SiO_4)_6O_3$ (Ln = La, Nd, Sm, Gd, Dy, Y, Ho, Er and Yb). *J. Mater. Chem.*, 1995, **5**, 1801–1806.
6. Nakayama, S. and Sakamoto, M., Electrical properties of new type high oxide ionic conductor $RE_{10}Si_6O_{27}$ (RE = La, Pr, Nd, Sm, Gd, Dy). *J. Eur. Ceram. Soc.*, 1998, **18**, 1413–1418.
7. Arikawa, H., Nishiguchi, H., Ishihara, T. and Takita, Y., Oxide ion conductivity in Sr-doped $La_{10}Ge_6O_{27}$ apatite oxide. *Solid State Ionics*, 2000, **136–137**, 31–37.
8. Nakayama, S. and Highchi, M., Electrical properties of apatite-type oxide ionic conductors $RE_{9.33}(SiO_4)_6O_2$ (RE = Pr, Nd and Sm) single crystals. *J. Mater. Sci. Lett.*, 2001, **13**, 913–915.
9. Nakayama, S. and Sakamoto, M., Ionic conductivities of apatite-type $La_x(GeO_4)_6O_{1.5x-12}$ (x = 8–9.33) polycrystals. *J. Mater. Sci. Lett.*, 2001, **20**, 1627–1629.
10. Tao, S. and Irvine, J. T. S., Preparation and characterisation of apatite-type lanthanum silicates by a sol–gel process. *Mater. Res. Bull.*, 2001, **36**, 1245–1258.
11. Abram, E. J., Sinclair, D. C. and West, A. R., A novel enhancement of ionic conductivity in the cation-deficient apatite $La_{9.33}(SiO_4)_6O_2$. *J. Mater. Chem.*, 2001, **11**, 1978–1979.
12. Tolchard, J. R., Islam, M. S. and Slater, P. R., Defect chemistry and oxygen ion migration in the apatite-type materials $La_{9.33}Si_6O_{26}$ and $La_8Sr_2Si_6O_{26}$. *J. Mater. Chem.*, 2003, **13**, 1956–1961.
13. Kharton, V. V., Shaula, A. L., Patrakeev, M. V., Waerenborgh, J. C., Rojas, D. P., Vyshatko, N. P. *et al.*, Oxygen ionic and electronic transport in apatite-type solid electrolytes. *J. Electrochem. Soc.*, 2004, **151**, A1236–A1246.
14. Tolchard, J. R., Sansom, J. E. H., Slater, P. R. and Islam, M. S., Effect of Ba and Bi doping on the synthesis and sintering of Ge-based apatite phases. *J. Solid State Electrochem.*, 2004, **8**, 668–673.
15. Sansom, J. E. H., Tolchard, J. R., Slater, P. R. and Islam, M. S., Synthesis and structural characterisation of the apatite-type phases $La_{10-x}Si_6O_{26+z}$ doped with Ga. *Solid State Ionics*, 2004, **167**, 17–22.
16. Sansom, J. E. H. and Slater, P. R., Oxide ion conductivity in the mixed Si/Ge apatite-type phases $La_{9.33}Si_{6-x}Ge_xO_{26}$. *Solid State Ionics*, 2004, **167**, 23–27.
17. Slater, P. R. and Sansom, J. E. H., The synthesis and characterisation of new apatite-type oxide ion conductors. *Solid State Phenom.*, 2003, **90–91**, 195–200.
18. Nakayama, S., Higuchi, Y., Kondo, Y. and Sakamoto, M., Effects of cation- or oxide ion-defect on conductivities of apatite-type La–Ge–O system ceramics. *Solid State Ionics*, 2004, **170**, 219–223.
19. Shaula, A. L., Kharton, V. V. and Marques, F. M. B., Oxygen ionic and electronic transport in apatite-type $La_{10-x}(Si,Al)_6O_{26\pm\delta}$. *J. Solid State Chem.*, 2005, **178**, 2050–2061.
20. Yaremchenko, A. A., Shaula, A. L., Kharton, V. V., Waerenborgh, J. C., Rojas, D. P., Patrakeev, M. V. *et al.*, Ionic and electronic conductivity of $La_{9.83-x}Pr_xSi_{4.5}Fe_{1.5}O_{26\pm\delta}$ apatites. *Solid State Ionics*, 2004, **171**, 51–59.
21. McFarlane, J., Barth, S., Swaffer, M., Sansom, J. E. H. and Slater, P. R., Synthesis and conductivities of the apatite-type systems, $La_{9.33+x}Si_{6-y}M_yO_{26+z}$ (M = Co, Fe, Mn) and $La_8Mn_2Si_6O_{26}$. *Ionics*, 2004, **8**, 149–154.
22. Shaula, A. L., Kharton, V. V., Waerenborgh, J. C., Rojas, D. P., Tsipis, E. V., Vyshatko, N. P. *et al.*, Transport properties and Mössbauer spectra of Fe-substituted $La_{10-x}(Si,Al)_6O_{26}$ apatites. *Mater. Res. Bull.*, 2004, **39**, 763–773.
23. Sansom, J. E. H., Sermon, P. A. and Slater, P. R., Synthesis and conductivities of the Ti doped apatite-type phases $(La/Ba)_{10-x}(Si/Ge)_{6-y}Ti_yO_{26+z}$. *Solid State Ionics*, 2005, **176**, 1765–1768.
24. Yoshikita, H. and Tanase, S., Magnesium doped lanthanum silicate with apatite-type structure as an electrolyte for intermediate temperature solid oxide fuel cells. *Solid State Ionics*, 2005, **176**, 2395–2398.
25. Rodriguez-Carvajal, J., Recent advances in magnetic structure determination by neutron powder diffraction. *Physica B*, 1993, **192**, 55–69.
26. Patrakeev, M. V., Mitberg, E. B., Lakhtin, A. A., Leonidov, I. A., Kozhevnikov, V. L., Kharton, V. V. *et al.*, Oxygen nonstoichiometry, conductivity and Seebeck coefficient of $La_{0.3}Sr_{0.7}Fe_{1-x}Ga_xO_{2.65+\delta}$ perovskites. *J. Solid State Chem.*, 2002, **167**, 203–213.
27. Kharton, V. V., Viskup, A. P., Figueiredo, F. M., Naumovich, E. N., Yaremchenko, A. A. and Marques, F. M. B., Electron–hole conduction in Pr-doped $Ce(Gd)O_{2-}$ by faradaic efficiency and emf measurements. *Electrochim. Acta*, 2001, **46**, 2879–2889.
28. Kharton, V. V., Shaula, A. L., Vyshatko, N. P. and Marques, F. M. B., Electron–hole transport in $(La_{0.9}Sr_{0.1})_{0.98}Ga_{0.8}Mg_{0.2}O_{3-\delta}$ electrolyte: effects of ceramic microstructure. *Electrochim. Acta*, 2003, **48**, 1817–1828.
29. Kharton, V. V. and Marques, F. M. B., Interfacial effects in electrochemical cells for oxygen ionic conduction measurements: I. The e.m.f. method. *Solid State Ionics*, 2001, **140**, 381–394.

30. Shannon, R. D., Revised effective ionic radii and systematic studies of interatomic distances in halides and chalcogenides. *Acta Crystallogr.*, 1976, **A32**, 751–767.
31. Kharton, V. V., Naumovich, E. N. and Vecher, A. A., Research on the electrochemistry of oxygen ion conductors in the former Soviet Union I. ZrO_2-based ceramic materials. *J. Solid State Electrochem.*, 1999, **3**, 61–81.
32. Takamura, H., Enomoto, K., Kamegawa, A. and Okada, M., Electrical conductivity of layered compounds in $SrO–La_2O_3–TiO_2$ systems prepared by the Pechini process. *Solid State Ionics*, 2002, **154–155**, 581–588.
33. Ahlgren, E. and Poulsen, F. W., Thermoelectric power of YSZ. *Solid State Ionics*, 1994, **70–71**, 528–532.
34. Naito, H. and Arashi, H., Electrical properties of $ZrO_2–TiO_2–Y_2O_3$ system. *Solid State Ionics*, 1992, **53–56**, 436–441.
35. Traquiera, L. S. M., Pagnier, T. and Marques, F. M. B., Structural and electrical characterization of titania-doped YSZ. *J. Eur. Ceram. Soc.*, 1997, **17**, 1019–1026.
36. Kharton, V. V., Viskup, A. P., Yaremchenko, A. A., Baker, R. T., Gharbage, B., Mather, G. C. *et al.*, Ionic conductivity of La(Sr)Ga(Mg,M)$O_{3-\delta}$ (M = Ti, Cr, Fe, Co, Ni): effects of transition metal dopants. *Solid State Ionics*, 2000, **132**, 119–130.